ACS Biomaterials SCIENCE & ENGINEERING

pubs.acs.org/journal/abseba
Article

Hybrid Biological Hydrogel Provides Favorable Bioenergetic, Adhesive, and Antioxidative Effects on Wound Healing

Xinyi Zhang, Zhijuan Hu, Ralf Pörtner, and An-Ping Zeng*

Cite This: https://doi.org/10.1021/acsbiomaterials.5c00072
Read Online

ABSTRACT: Wound healing is a dynamic and complex process that demands substantial energy expenditure and a biomimetic microenvironment. Developing a simple and effective biological hydrogel to enhance mitochondrial energy metabolism could effectively promote wound healing. To this end, we developed a hybrid biological hydrogel based on *Escherichia coli* lipoate protein ligase A (LplA), which combines its catalytic and self-assembling properties to promote wound healing. In murine fibroblast L929 cell models, LplA significantly enhances cellular activity and intracellular metabolism, promoting cell proliferation and energy supply. However, cells aggregated into spherical clusters on the pure LplA hydrogel. To address this issue, we integrated glutaraldehyde (GA) as a cross-linker into the LplA hydrogel. The GA-LplA hydrogel enhances cell adhesion and proliferation and, unexpectedly, exhibits higher catalytic activity compared with the pure LplA hydrogel. Furthermore, LplA was observed to decompose H_2O_2, and the GA-LplA hybrid hydrogel significantly reduced reactive oxygen species (ROS) production. The promise of this hybrid hydrogel is successfully demonstrated in a male mice full-thickness skin defect model with accelerated re-epithelialization and cell proliferation while reducing inflammation.

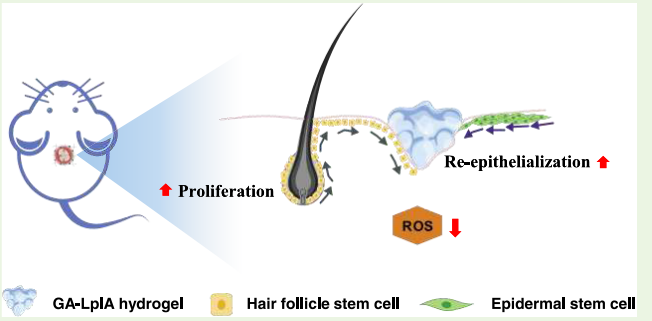

KEYWORDS: *LplA, protein hydrogel, energy metabolism, antioxidant, cell proliferation, wound healing*

1. INTRODUCTION

Wound healing is an essential yet complex process in humans and animals, involving several stages: inflammation, proliferation, and remodeling.[1,2] This process is highly dynamic and energy-demanding.[3] Mitochondria serve as the primary site of biological energy production, converting substrates into ATP.[4] Increased reactive oxygen species (ROS) during the wound healing period have been reported to induce mitochondrial dysfunction, thereby reducing ATP production and delaying wound healing.[5] Rescuing or compensating for mitochondrial function has been proven to be an effective therapeutic strategy in wound healing.[6] The direct intracellular delivery of ATP can enhance incisional wound healing, reduce surgical wound dehiscence, and promote rapid tissue regeneration in acute wound healing.[7,8] Thylakoid membrane-encapsulated polyphenol nanoparticles (PTKM NPs) were reported to generate ATP and NADPH, thus enhancing mitochondrial function and promoting chronic wound healing.[9] Besides, hydrogels, particularly functional hydrogels, which create biomimetic microenvironments to stimulate cell proliferation and mitigate inflammation, are reported to expedite wound healing.[10] In a murine model of infected wounds, the GSC/PBE@Lut hydrogel exhibits significant therapeutic benefits through its antibacterial, anti-inflammatory, angiogenic, and tissue regenerative effects. This smart material achieves these outcomes, controllably releasing Cu to promote angiogenesis and luteolin to exert anti-inflammatory actions.[11] Given the pivotal role of fibroblasts in wound healing, the murine fibroblast (L929) cell model has been widely utilized to develop medical materials. A proangiogenic peptide nanofiber hydrogel was reported to enhance the adhesion and proliferation of L929 and human umbilical vein endothelial cells (HUVECs) *in vitro*.[12] A bFGF and collagen matrix hydrogel was designed to promote the proliferation of L929 cells, thereby accelerating the healing of burn injuries in Wistar rats.[13] Additionally, glutaraldehyde (GA) is commonly employed as a cross-linker in hydrogel preparation to improve its mechanical properties and stability.[14] Therefore, an easy-to-prepare material that simultaneously enhances cellular mitochondrial energy metabolism and provides a moist healing environment is highly desired for wound healing.

LplA, a functional protein derived from *Escherichia coli*, directly utilizes lipoate to complete the lipoylation process.[15,16]

Received: January 10, 2025
Revised: April 7, 2025
Accepted: April 24, 2025

This process is a highly conserved post-translational modification from bacteria to humans, which is crucial for regulating mitochondrial metabolism-related enzyme complexes, including pyruvate dehydrogenase (PDH), α-ketoglutarate dehydrogenase (KGDH), branched-chain α-ketoacid dehydrogenase (BCKDH), 2-oxoadipate dehydrogenase (OADH), and glycine cleavage system (GCS).[17,18] Among these, PDH and OGDH are crucial in the TCA cycle, whereas BCKDH, OADH, and GCS play significant roles in the catabolism of branched-chain amino acids (valine, leucine, isoleucine), lysine, and glycine, respectively. In all of these complexes, a specific subunit is modified by the attachment of lipoate to the specific lysine residues within conserved lipoyl domains. Consequently, lipoylation is essential for both mitochondrial energy metabolism and amino acid metabolism. Dysregulation of the lipoylation process can result in an inadequate energy supply and metabolic imbalance. Emerging evidence indicates that LplA can effectively mitigate lipoate deficiency in mammalian cells, thereby treating mitochondrial dysfunction and enhancing energy metabolism. The overexpression of LplA in human cell models of lipoylation deficiency could recover their lipoylation levels and cellular respiration.[19] Our group demonstrated the rescue effect of LplA in human cells and extended this finding to mouse models.[20] Besides, we discovered that LplA exhibits self-assembly properties *in vitro*, forming a responsive hydrogel while retaining its catalytic functions.[21,22] More recently, Wang et al. developed a promising synthetic biology tool leveraging the phase-separation properties of LplA *in vivo*.[23] This tool facilitates the rational design of synthetic condensates with distinct subcellular localizations and translocations, offering a practical alternative for constructing ligand-responsive genetic switches that modulate gene expression at various levels. Given its crucial role in mitochondrial energy metabolism and its self-assembly features, LplA may represent a novel "simple but effective" material for wound healing.

In this study, we investigated the potential of LplA hydrogels for wound healing. The biocompatibility of LplA was assessed using L929 cells, and its effects on cellular metabolism were explored through both intracellular expression and the extracellular addition of LplA. Unexpectedly, L929 cells showed poor adhesion on LplA hydrogels. To solve this problem, a glutaraldehyde (GA)-LplA hybrid hydrogel was developed. The GA-LplA hydrogel was subsequently evaluated in an *in vitro* H_2O_2-induced oxidative damage cell model and in an *in vivo* full-thickness skin defect mice model. As a material with a simple composition and easy preparation, GA-LplA hydrogel has the potential to provide a biomimetic microenvironment throughout the wound healing process, enhance energy metabolism, exhibit antioxidant properties, and promote re-epithelialization, thereby accelerating wound healing.

2. MATERIALS AND METHODS

2.1. Materials. The adherent growing cell line L929 (NCTC clone 929, CCL-1TM) was obtained from ATCC (Manassas, VA). The HEK293T cell line was sourced from the National Collection of Authenticated Cell Cultures (Serial No. SCSP-502). Phosphate-buffered saline (PBS) solution was purchased from Carl Roth GmbH (Karlsruhe, Germany). Dulbecco's modified Eagle's medium (DMEM) was obtained from PAN-Biotech (Aidenbach, Germany), and Gibco Roswell Park Memorial Institute (RPMI 1640) medium was sourced from Thermo Fisher Scientific (Waltham, MA). Penicillin/streptomycin was acquired from Corning (Kennebunk, ME), while trypsin was obtained from the Lonza Group AG (Basel, Switzerland). Glutaraldehyde, glycine, NaCl, lipoic acid, ATP, and $MgCl_2$ were obtained from Sigma-Aldrich (St. Louis, MO), while the collagen standard was purchased from Merck (Millipore Sigma, St. Louis, MO).

2.2. Production and Purification of LplA. The gene encoding *E. coli* LplA was constructed in pET-28a (+) vectors using In-Fusion cloning. Proteins were produced by cultivating the bacterium *E. coli* BL21(DE3) in LB medium and subsequent purification following the procedure described by Zhang et al.[24] In brief, recombinant cells were incubated in LB medium containing 50 μg/mL kanamycin at 37 °C until the OD_{600} reached about 0.6. Protein expression was induced by adding 0.2 mM Isopropyl-β-D-Thiogalactoside (IPTG) and incubating for 8 h at 30 °C. Cells were harvested by centrifugation at 10,000*g* for 10 min at 4 °C. The cell pellets were resuspended in lysis buffer (300 mM NaCl, 50 mM Tris-HCl, 20 mM imidazole, pH 7.5) and lysed using an Ultrasonic Crusher. Following centrifugation, the lysate was loaded onto a Ni^{2+} chelating Sepharose Fast Flow column (GE Healthcare, Uppsala, Sweden) for purification via FPLC. The purified protein solution was then treated with an endotoxin removal kit (Thermo Scientific) to eliminate endotoxins. The purity of the recovered proteins was assessed by using 12% sodium dodecyl sulfate-polyacrylamide gel electrophoresis (SDS-PAGE).

2.3. Effect of LplA on L929 Cells. *2.3.1. Biocompatibility Assay.* Cell viability in cultures with different concentrations of LplA (0−10 mg/mL) was measured to assess the biocompatibility of LplA. L929 cells were cultured in RPMI 1640 medium supplemented with 10% bovine serum and 1% penicillin/streptomycin. Cells were seeded on 96-well plates at a density of 10,000 cells/cm^2 and incubated at 37 °C with 5% CO_2. After 24 h, the culture supernatant was replaced with fresh medium containing LplA (0−10 mg/mL) and incubated for an additional 72 h. Cell viability was assessed using the neutral red uptake (NRU) assay, CCK-8 kit (Sigma-Aldrich), and resazurin kinetic assay, following the manufacturer's instructions. Untreated cells served as the control for 100% cell viability. Each assay was performed in duplicate with a sample size of $N = 5$ per group.

2.3.2. Intracellular Energy Metabolism Assay. To analyze intracellular energy metabolism, we measured the $NADH/NAD^+$ ratio and ATP levels in cells treated with LplA. L929 cells were cultured in RPMI 1640 medium supplemented with 10% bovine serum and 1% penicillin/streptomycin in 96-well plates. After 24 h, the culture supernatant was replaced with fresh medium containing LplA (0−10 mg/mL), and the cells were incubated for an additional 72 h. ATP levels were quantified using the ATP Assay Kit (Abcam, US), and the $NADH/NAD^+$ ratio was measured using the NAD/NADH Assay Kit (Abcam, US). Each group included $N = 5$ samples, and the studies were performed in duplicate.

2.3.3. Measurement of Glucose Consumption and Lactate Production. The cells were treated according to the methodology described in Section 2.3.2. Following a 72 h incubation period, the supernatant was collected to measure glucose and lactate concentrations. These concentrations were quantified using a YSI 2900 biochemical analyzer (YSI Life Sciences, Simpsonville, SC).

2.3.4. Cell Mitochondrial Stress Assay. Mitochondrial targeting sequence (MTS) was used for the localization of LplA in the mitochondrial matrix. The MTS of ornithine transcarbamylase (Uniprot, P00480) was synthesized by Genscript (Nanjing, China). Fragments of MTS, GFP, and LplA were inserted into the pCDH-CMV vector (Addgene, 72265) by using In-Fusion cloning. LplA-overexpressing L929 cell lines were generated by lentivirus transfection with the corresponding plasmids. Oxygen consumption rate (OCR) was measured using an XFe96 extracellular flux analyzer (Agilent). L929 cells were seeded at a density of 10,000 cells per well and incubated for 24 h. Before the assay, cells were equilibrated for 1 h in a non-CO_2 incubator with XF Base medium supplemented with 10 mM glucose, 2 mM pyruvate, and 4 mM L-glutamine. OCR was measured by sequentially injecting 1 μM oligomycin, 1 μM FCCP, and 1 μM rotenone/1 μM antimycin A. Mitochondrial function was assessed based on basal respiration and ATP production.

https://doi.org/10.1021/acsbiomaterials.5c00072
ACS Biomater. Sci. Eng. XXXX, XXX, XXX−XXX

2.3.5. Determination of H_2O_2 Degradation Activity. The ability of LplA to degrade H_2O_2 was assessed by measuring O_2 production using a sensor dish reader (SDR, Presens, Germany). In the reaction system, 0.6 mg/mL LplA was mixed with varying concentrations of H_2O_2 (0−20 mM) and incubated at 37 °C.

2.4. Preparation and Characterization of Hydrogels. *2.4.1. Preparation of Hydrogels. 2.4.1.1. LplA Hydrogel.* The LplA protein was dialyzed against PBS using a 20 mL dialysis cassette (Thermo Fisher, Slide-A-Lyzer, 30 kDa) at 4 °C overnight. Subsequently, endotoxins were removed using an endotoxin removal kit (Thermo Scientific). The concentration of the purified protein was measured using a NanoDrop spectrophotometer. The purified proteins were then diluted with a precold buffer to a concentration of 40 mg/mL and incubated at 37 °C for 5 min to form LplA hydrogels.

2.4.1.2. GA-LplA Hydrogel. The LplA solution was diluted to a concentration of 20 mg/mL in PBS. The LplA solution was then thoroughly mixed with 0.55 wt % glutaraldehyde (GA) and incubated at 37 °C for 5 min. Subsequently, the solution was immersed in an 8 wt % glycine solution to neutralize the free aldehyde groups in glutaraldehyde. After 4 h, the supernatant was discarded, and the remaining hydrogel was washed three times with PBS, resulting in the formation of the GA-LplA hydrogel.

2.4.2. Characterization of the Structural and Catalytic Properties of Hydrogels. 2.4.2.1. Rheology Measurements. The rheological analysis of the GA-LplA hydrogel was determined using a rotational rheometer (AR2000ex, TA Instruments) equipped with a parallel palate (40 mm diameter). Strain scanning of the GA-LplA hydrogel was performed over a range of 0.1%−1000%. Frequency sweep measurements of the GA-LplA hydrogel were conducted at a constant strain of 1%.

2.4.2.2. Structural Properties. The surface morphology of the lyophilized hydrogels was examined by using a scanning electron microscope (SEM) (Zeiss Gemini 450). The prepared hydrogels were rapidly immersed in liquid nitrogen and subsequently lyophilized. After being dried, the samples were transferred to a carbon adhesive-covered sample stage and coated with a gold layer via sputtering. The surface morphology was observed by using SEM.

2.4.2.3. Catalytic Properties. The experimental conditions for evaluating the catalytic ability of the hydrogels (LplA hydrogel and GA-LplA hydrogel) are outlined in Table 1. 100 μL hydrogels were immersed in a 1 mL reaction solution. The reaction was initiated by adding ATP, and the mixture was incubated at 37 °C for the specified durations. The supernatant was collected to measure the concentrations of lipoylated H-protein (H_{lip}) using a previously established high-performance liquid chromatography (HPLC) method.[25]

Table 1. Reaction System for Hydrogel Catalytic Ability Determination

component	concentration
R-(+)-lipoic acid	0.5 mM
ATP	1.0 mM
$MgCl_2$	2.0 mM
DTT	0.1 mM
H_{apo}	40 μM

2.5. Performance of L929 Cells on Hydrogels. *2.5.1. Cell Adhesion Assay.* L929 cells were cultured until they reached 80−90% confluence, after which they were trypsinized and harvested. Then, 50 μL of collagen hydrogel, LplA hydrogel, and GA-LplA hydrogel were added separately to the wells of a 96-well plate and incubated for 5 min to facilitate hydrogel formation. A suspension of 50,000 cells in 150 μL of the medium was then added to each well, and the cells were allowed to attach for 4 h at 37 °C. Following this, the cells were washed twice with PBS to remove nonadherent cells, and cell numbers were quantified using the CCK-8 assay kit. The experiments were conducted in triplicate. The control group did not receive the hydrogel treatment.

2.5.2. Staining of Live/Dead Cells. The biocompatibility of the hydrogels with L929 cells was assessed using live/dead staining assays. Cells were seeded onto various hydrogels in 48-well plates at an initial density of 5000 cells/cm^2 and incubated at 37 °C with 5% CO_2. After 48 h of incubation, live and dead cells were distinguished using Calcein-AM and propidium iodide staining. The final concentration of Calcein-AM and propidium iodide in the medium was 2 μM, and cells were incubated at 37 °C for an additional 15 min. Live and dead cells were visualized by using a Nikon fluorescence microscope.

2.5.3. Cell Proliferation Assay. Hydrogels were introduced into a 48-well plate, followed by the seeding of L929 cells at an initial density of 5000 cells/cm^2. The cells were then incubated at 37 °C in 5% CO_2. After 72 h, cell proliferation was quantified using a CCK-8 assay kit. The proliferation rate of the control group, which did not receive hydrogel treatment, was designated as the 100% reference value.

2.5.4. Cell Migration Assay. The migration of L929 cells across various hydrogels was investigated by using an *in vitro* scratch assay. Hydrogels were introduced into 12-well plates, and the Culture-Insert 2 Well (Ibidi, Munich, Germany) was placed onto the hydrogel surface. 70 μL cell suspension (300,000 cells/mL) was added to each well of the culture insert. After 24 h, a confluent cell layer was obtained. The Culture-Insert 2 Well was then gently removed using sterile tweezers, and the cell layer was washed with PBS to remove cell debris and nonadherent cells. Cell migration across a 500 μm cell-free gap was subsequently observed.

2.5.5. Intracellular ROS Assay. L929 cells were seeded onto 96-well plates at a density of 10,000 cells per well and incubated following the protocol described in Section 2.5.2. After 48 h, the supernatant was removed, and the wells were replenished with 100 μL of medium containing 100 μM H_2O_2, followed by a 4 h incubation. The supernatant was then discarded, and the cell layer was gently washed with PBS. Subsequently, cells were incubated with 10 μM DCFH-DA for 30 min at 37 °C, and intracellular ROS levels were measured via fluorometric detection at an excitation/emission wavelength of 485/522 nm. The intensity of DCF fluorescence is directly proportional to the quantity of intracellular ROS generated. Data were presented as percentages relative to control values. The capacity for reuse of the GA-LplA hydrogel in degrading H_2O_2 was quantified by using the peroxide-test kit (Merck, Darmstadt, Germany).

2.6. *In Vivo* Wound Healing Study. *2.6.1. Full-Thickness Skin Defect Model.* Male C57BL/6J mice (8 weeks old) were purchased from Charles River (Zhejiang, China). All animal studies adhered to the guidelines of the Laboratory Animal Resources Center at Westlake University. Full-thickness skin defects, 6 mm in diameter, were created on the back of mice and treated with GA-LplA hydrogel. The wounds treated with PBS were used as the control group. Each group consisted of three mice. Hydrogels were applied to the wounds post-surgery. In detail, the wound surface was completely covered with hydrogel, which was cleaned and replaced with fresh hydrogel every 2 days. The control group was washed with PBS. The wound healing process was documented by photographing the wounds on Days 0, 2, 4, 6, and 12 after treatment. The wound contraction ratio was calculated as follows:

$$\text{wound contraction ratio} = (A_i - A_t)/(A_i) \times 100\%$$

where A_t is the area of the wound at day t and A_i is the initial area of the wound. Mice were euthanized 12 days after treatment. The healing process was monitored using a digital camera, and the wound area was quantified by using ImageJ software.

2.6.2. H&E Staining and Immunofluorescence Staining. Collagen hydrogel was added as an additional control to the above-mentioned model, with the dressing changed daily. On days 4 and 8, animals were weighed and then euthanized; wound tissues were collected. The tissues were fixed in 4% Paraformaldehyde for 15 min, dehydrated, embedded in optimum cutting temperature compound, and stored in −80 °C before analysis. OTC-embedded samples were sectioned at 5 μm. The slides were stained with hematoxylin and eosin (H&E) staining. Images were captured using a laser scanning confocal

https://doi.org/10.1021/acsbiomaterials.5c00072
ACS Biomater. Sci. Eng. XXXX, XXX, XXX−XXX

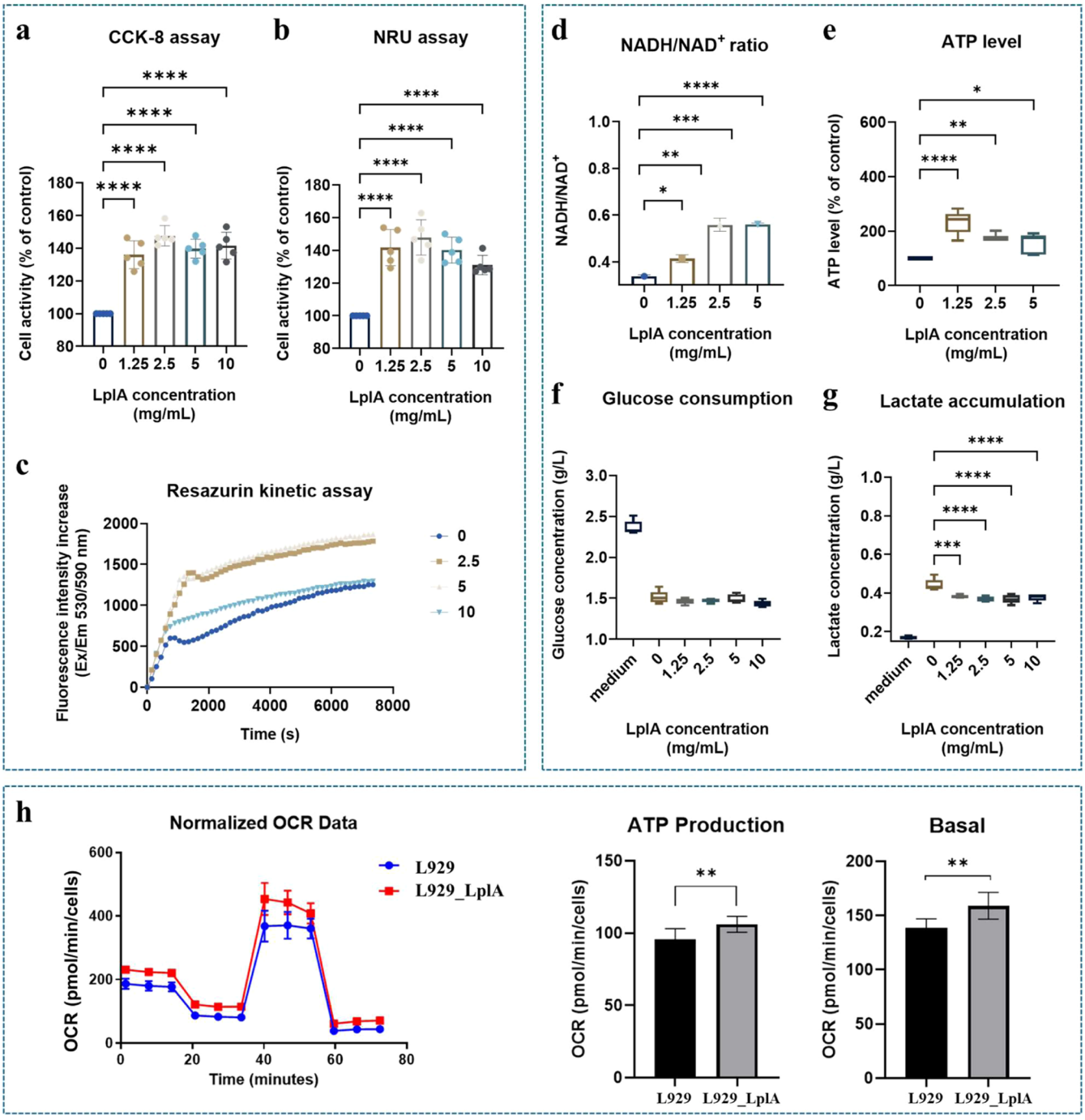

Figure 1. Effect of LplA on the activity and metabolism of L929 cells. (a, b) Cell activity assay using the neutral red uptake and CCK-8 kit, respectively; (c) cell activity assay using resazurin kinetic assay; (d) NADH/NAD$^+$ ratio quantitative analysis; (e) ATP level quantitative analysis; and (f, g) quantitative analysis of glucose consumption and lactic acid accumulation. (h) Quantitative analysis of cellular oxygen consumption rate (OCR) in L929 wild type and LplA-overexpressing cell lines; (i) calculation of ATP production and basal respiration for OCR. All data are shown as the mean ± error standard of n = 5 independent experiments. Filled circles show individual results (n). Statistical significance was determined using a two-tailed, unpaired Student's t test. *, $p < 0.05$; **, $p < 0.01$; ***, $p < 0.001$; ****, $p < 0.0001$; ns, not significant.

microscope (LSM980). Moreover, immunofluorescence staining (EDU, K14, CD11b) was employed to evaluate skin tissue regeneration, and nuclei were stained with DAPI.

2.7. Statistics and Reproducibility. Statistical analysis was performed using GraphPad Prism (v9.0). Differences between any two groups were analyzed using a two-tailed, unpaired Student's t test. For comparisons involving more than two groups, one-way ANOVA with Tukey's multiple comparisons was employed. $P < 0.05$ was considered statistically significant. The presented data indicates the mean ± SD from at least two independent experiments.

3. RESULTS AND DISCUSSION

3.1. Effect of LplA on the Activity and Metabolism of L929 Cells. LplA with a purity of over 80% (Figure S1) was obtained by nickel ion affinity chromatography. Endotoxin from *E. coli* was removed by 97.59% (Table S1). Other physicochemical properties of LplA are summarized in Table S2. To investigate the biocompatibility of LplA, the purified LplA protein was dissolved in the medium used for cultivating

https://doi.org/10.1021/acsbiomaterials.5c00072
ACS Biomater. Sci. Eng. XXXX, XXX, XXX−XXX

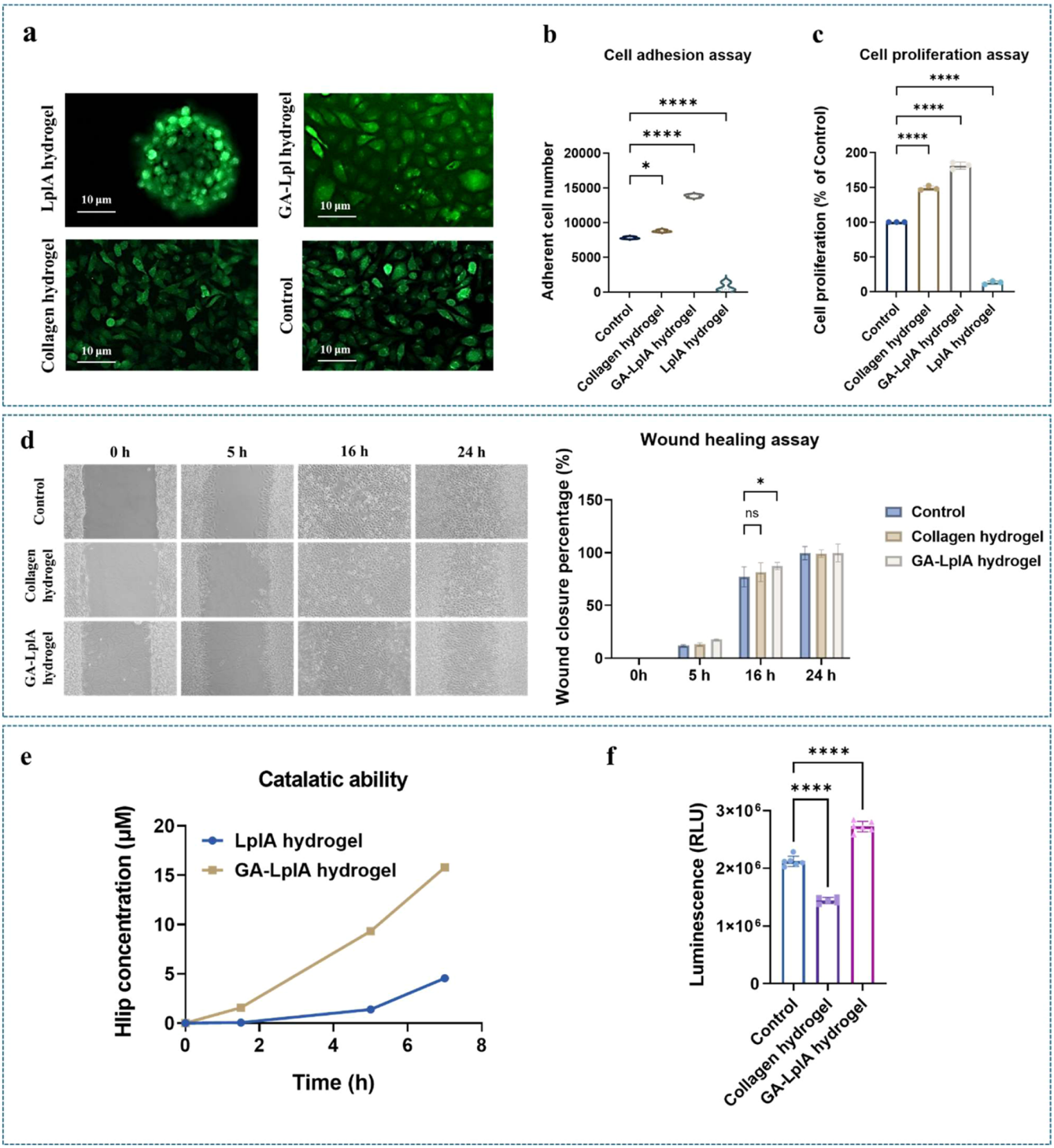

Figure 2. Functional assays of cells on hydrogels and characterization of gel properties. (a) Cell adhesion ability on different matrixes (scale bar: 10 μm); (b) quantitative analysis of cell adhesion on different matrixes; (c) cell proliferation ability on different matrixes; (d) comparison of cell migration abilities on different matrixes using wound healing assay; (e) catalytic activity of GA-LplA hydrogel and LplA hydrogel; and (f) quantification of ATP levels of L929 cells on different hydrogels. All data are shown as the mean ± error standard of n = 3 independent experiments. Statistical significance was determined using a two-tailed, unpaired Student's t test. *, $p < 0.05$; **, $p < 0.01$; ***, $p < 0.001$; ****, $p < 0.0001$; ns, not significant.

L929 cells at different concentrations. The cultures were then analyzed by employing NRU, CCK-8, and resazurin kinetic assays. The NRU assay evaluated the dye absorption capability of lysosomes within the cells,[26] while the CCK-8 and resazurin kinetic assays quantified the reductive activity of intracellular dehydrogenases.[27,28] Compared to the LplA-free control group (Figure 1a–c), LplA supplementation at concentrations of 2.5 and 5 mg/mL markedly increased cell activity by 120–150%. These findings indicated that LplA exhibits good biocompatibility, and moderate concentrations of LplA enhance cell activity, potentially due to its catalytic properties that boost cellular metabolism. However, at an LplA concentration of 10

https://doi.org/10.1021/acsbiomaterials.5c00072
ACS Biomater. Sci. Eng. XXXX, XXX, XXX−XXX

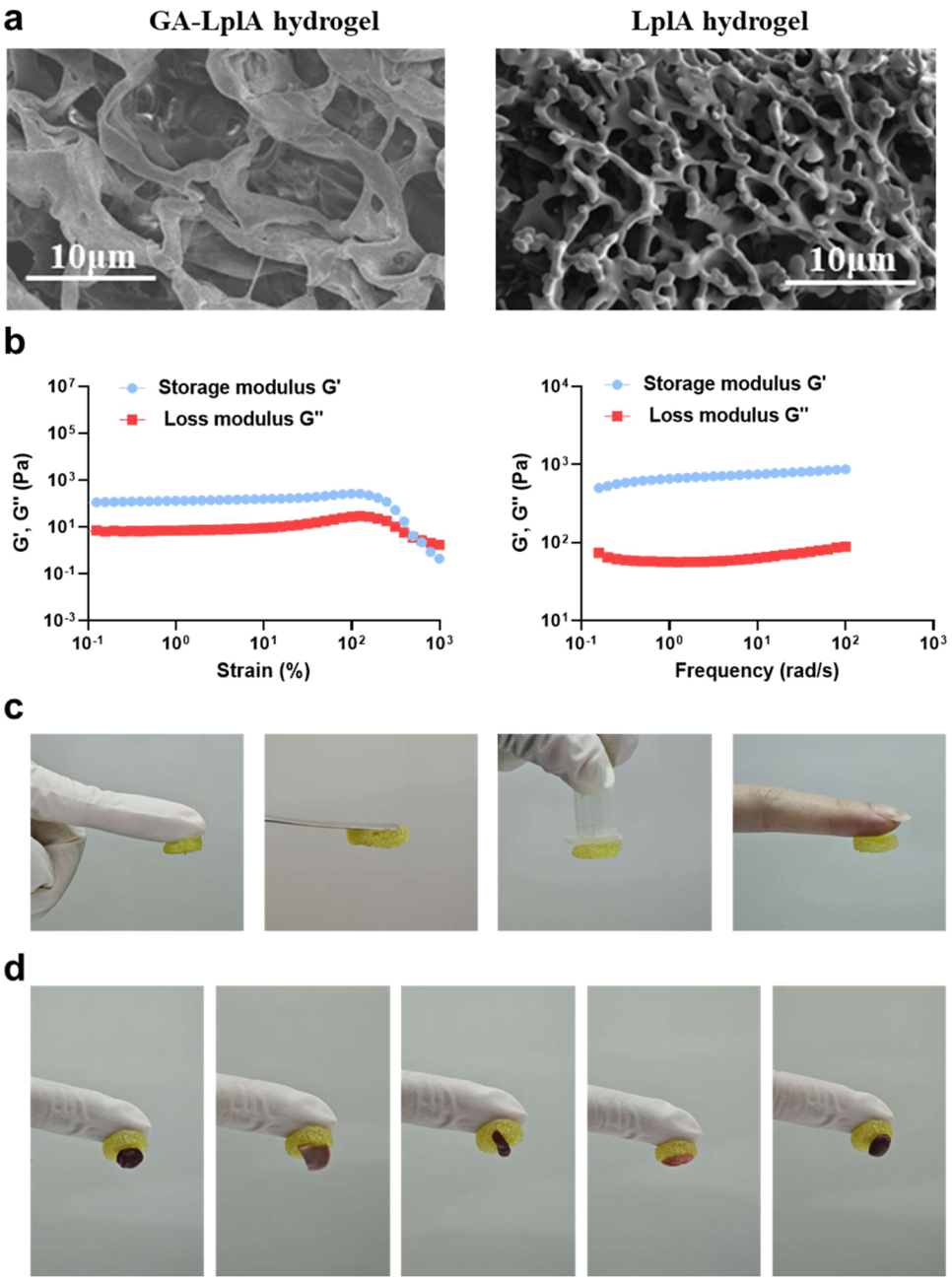

Figure 3. Characterization of the gel properties. (a) SEM images of GA-LplA hydrogel and LplA hydrogel (scale bar: 10 μm); (b) strain scanning of GA-LplA hydrogel in the range of 0.1−1000%. Frequency sweep of GA-LplA hydrogel at a constant strain (1%); (c) adhesive capacity of GA-LplA hydrogel on different substrates; and (d) adhesion of GA-LplA hydrogel to mouse organs (from left to right: heart, liver, spleen, lung, and kidney).

mg/mL, a discernible reduction in cell activity was observed compared to lower concentrations. LplA is reported to form hydrogels spontaneously at 40 mg/mL,[29] and at 10 mg/mL, it can self-assemble into aggregates that induce significant turbidity in culture medium. Consequently, the aggregation of LplA at 10 mg/mL may interfere with oxygen transfer, nutrient uptake, and waste elimination, thereby negating the positive impact of LplA on cellular activity.

Cell activity is intricately linked to intracellular energy metabolism. To evaluate the enhancement of cellular activity by LplA, as measured by NRU, CCK-8, and resazurin kinetic assays, we quantified the NADH/NAD^+ ratio, ATP levels, glucose consumption, and lactate accumulation. Figure 1d,e shows that LplA concurrently increased the NADH/NAD^+ ratio and intracellular ATP levels, indicating a potential enhancement in cell activity through improved energy metabolism. Moreover, glucose consumption remained at a similar level (Figure 1f), while the diminished lactate production observed in Figure 1g suggests that LplA might promote intracellular ATP synthesis by redirecting cellular metabolism toward aerobic respiration. These results support the hypothesis that LplA may enhance aerobic respiration, thereby increasing ATP synthesis and cell activity. It is proposed that this effect is due to the internalization of the LplA protein into the cells, where it performs a catalytic function, thus inducing a metabolic change. To investigate

https://doi.org/10.1021/acsbiomaterials.5c00072
ACS Biomater. Sci. Eng. XXXX, XXX, XXX−XXX

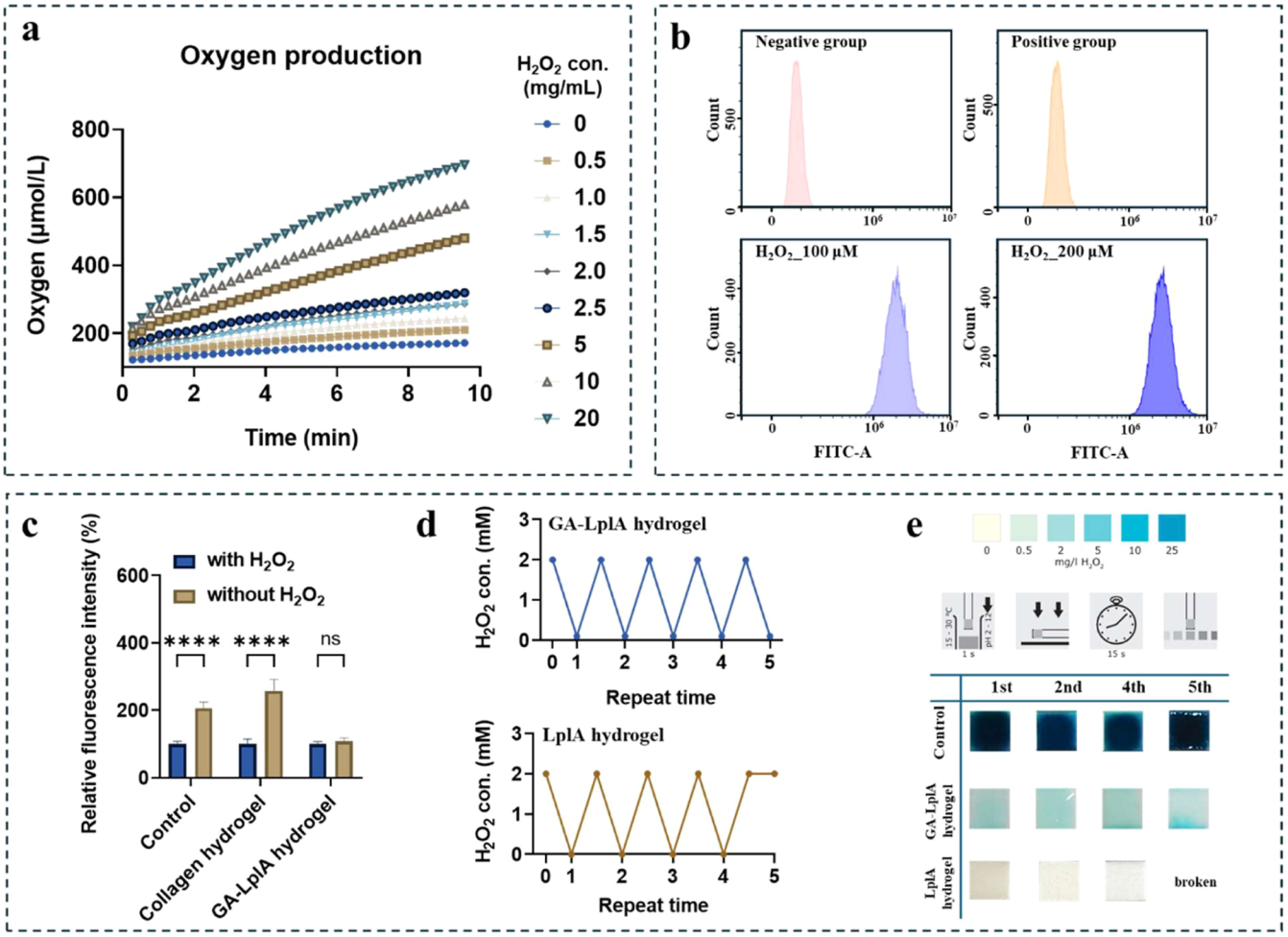

Figure 4. Antioxidant properties and reusability of the GA-LplA hydrogel. (a) Oxygen production rate of LplA decomposition of different H_2O_2 concentrations; (b) H_2O_2 induced oxidative damage efficiency in cells, measured by flow cytometry; (c) H_2O_2 induced oxidative damage efficiency in cells on different matrixes; (d) quantitative analysis of the reusability of LplA hydrogel and GA-LplA hydrogel; and (e) qualitative analysis of the reusability of LplA hydrogels and GA-LplA hydrogels. All data are shown as the mean ± error standard of $n = 3$ independent experiments. Statistical significance was determined using one-way ANOVA with Tukey's multiple comparisons. *, $p < 0.05$; **, $p < 0.01$; ***, $p < 0.001$; ****, $p < 0.0001$; ns, not significant.

whether LplA is internalized into the cells, we conducted Western blot analysis (Figure S2). After coculturing L929 cells with 2.5 mg/mL LplA for 48 and 72 h, cells were washed with ice-cold PBS three times and lysed with RIPA buffer. LplA was detected in the supernatant of the cell lysates using anti-LplA antibody, indicating that a portion of LplA may be internalized into cells and exert intracellular effects.

To further investigate the impact of LplA on intracellular energy metabolism in L929 cells, we introduced heterologous expression of LplA in L929 cell lines and evaluated changes in cellular energy metabolism using a mitochondrial stress test. Data presented in Figure 1h indicated that the expression of LplA led to a significant increase in the basal respiratory capacity of L929 cells, along with a rise in intracellular ATP concentrations. These observations align with the outcomes from extracellular assays, indicating that the increase in cell activity is indeed attributed to LplA.

3.2. Cell Functional Assays on Hydrogels and Characterization of Gel Properties. Given the notable efficacy of LplA in enhancing cellular activity and its inherent gelation capability, we evaluated its potential as a material to promote wound healing using the L929 cell model. The cytotoxicity of hydrogels was assessed using the CCK-8 kit following a 48 h coculture with hydrogel extracts. The results showed that the cell viability of the GA-LplA hydrogel and collagen hydrogel groups did not significantly differ from that of the control group, indicating that they have good biocompatibility and suitability for further *in vivo* or *in vitro* applications (Figure S3). The adhesion of L929 cells to LplA hydrogels was assessed by seeding the cells on the hydrogel surface and examining the cell morphology through fluorescence microscopy. Observations revealed that cells failed to adhere to the LplA hydrogel surface and instead aggregated into spherical clusters (Figure 2a). Notably, these clusters consisted of living cells, as indicated by live/dead staining visualized by fluorescence microscopy (Figure 2a). The formation of spherical clusters by L929 cells on the LplA hydrogel may be attributed to its excessively soft texture, which creates a low-adhesion surface that promotes spheroid formation.[30,31] Conversely, L929 cells demonstrated effective adhesion to the commercial collagen hydrogel, as evidenced in Figure 2a.

To address this limitation and further improve the performance of LplA hydrogel, we examined a hybrid hydrogel

https://doi.org/10.1021/acsbiomaterials.5c00072
ACS Biomater. Sci. Eng. XXXX, XXX, XXX−XXX

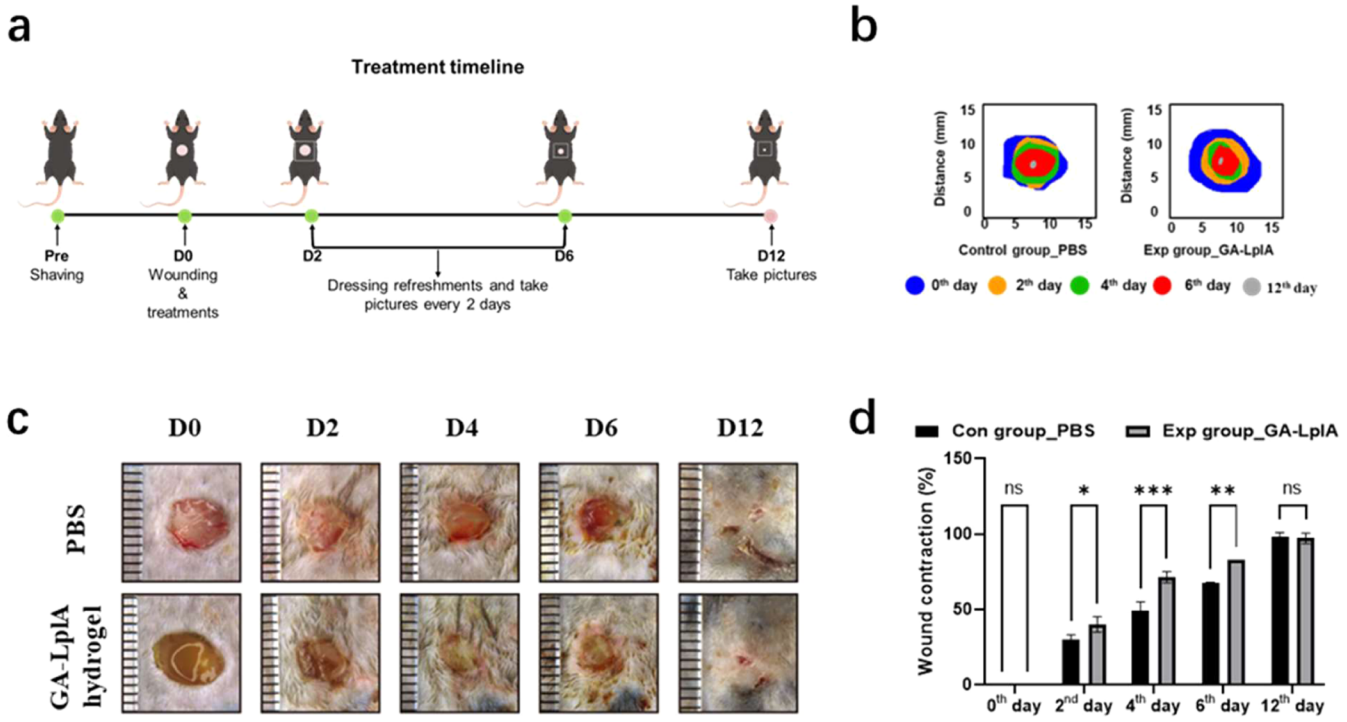

Figure 5. *In vivo* efficacy of GA-LplA hydrogel in a mouse full-thickness skin defect model. (a) Illustration of wound creation and treatment timeline; (b) traces of wound closure from day 0 to day 12; (c) digital images of the wound bed in all treatment groups on days 0, 2, 4, 6, and 12; (d) quantitative visualization of percentage wound closure for all groups at the same time points as in panel (c). Statistical significance was determined using one-way ANOVA with Tukey's multiple comparisons. *, $p < 0.05$; **, $p < 0.01$; ***, $p < 0.001$; ns, not significant.

with glutaraldehyde (GA) cross-linked with LplA. As a cross-linking agent, GA was reported to improve the mechanical stability of hydrogels and enhance cell adhesion in previous studies.[23,25] Indeed, L929 cells successfully adhered to the GA-LplA hydrogel, with adhesion levels comparable to those on the collagen hydrogel (Figure 2b). Moreover, no instances of cell death were detected after 6 h, as confirmed by the live/dead staining assay.

Promoting cell proliferation is a critical attribute for hydrogels used as substrates in cell culturing and wound healing. We assessed cell proliferation efficiency across various hydrogels using the CCK-8 assay, with the untreated group serving as the benchmark. As depicted in Figure 2c, L929 cells exhibited significant proliferation within the commercial collagen hydrogel, achieving 147% relative to that of the control. In strong contrast, the LplA hydrogel failed to support comparable cell proliferation, demonstrating only 10% of the control group's rate. On the other hand, cells cultured on the GA-LplA hydrogel showed enhanced proliferation, reaching 170% of the control group's rate. This enhancement is likely due to the improved cell adhesion properties conferred by the GA-LplA hydrogel and the beneficial effects of LplA on intracellular metabolism, which may facilitate accelerated cell growth. Importantly, the density of adherent cells per well on the GA-LplA hydrogel exceeded that observed on the collagen hydrogel (Figure 2b), suggesting the GA-LplA hydrogel's superior capacity to support cell adhesion and proliferation. The ATP levels of cells on various hydrogels were measured, and the results indicated that cell viability on the GA-LplA hydrogel was significantly higher than those on the control and collagen hydrogel groups (Figure 2f). Consequently, GA-LplA hydrogels are recognized as promising materials for enhancing cell adhesion, proliferation, and energy metabolism in future research endeavors. Figure 2d illustrates that both GA-LplA and collagen exhibited a slight enhancement in promoting cell migration compared with the control group. Specifically, at the 16 h time point, the migration rate in the GA-LplA group was slightly higher than that in the collagen group.

LplA, a natural ligase, catalyzes the lipoylation of the H-protein from H_{apo} to H_{lip}. The GA-LplA hydrogel is produced through a cross-linking reaction that employs glutaraldehyde, which may potentially affect the ligase's catalytic function. Intriguingly, the cross-linking hydrogel demonstrated a higher lipoylation catalytic ability compared to that of the pure LplA hydrogel, as shown in Figure 2e. It is hypothesized that in the unmodified LplA hydrogel, which relies on spontaneous self-assembly of LplA molecules, conformational alterations may compromise catalytic efficiency. Conversely, in the GA-LplA hydrogel, cross-linking facilitates the formation of a structurally supportive framework, potentially stabilizing each LplA molecule in a conformation that enhances its inherent catalytic activity.

Moreover, the SEM image of the hydrogel formulations (Figure 3a) revealed that the GA-LplA hydrogel has a higher pore size than that of the pure LplA hydrogel (Figure S4). Besides, GA-LplA also possesses injectable properties (Figure S5). Strain scanning and frequency sweep (Figure 3b) demonstrate that the storage modulus (G') and loss modulus (G'') of the GA-LplA hydrogel are superior to those of the LplA hydrogel.[20] Adhesion properties of the GA-LplA hydrogel were investigated on various materials and tissues, including rubber, steel, plastic, skin, and multiple mouse organs (Figure 3c,3d). The results showed that the GA-LplA hydrogel adhered tightly to the surfaces of all of the tested materials and organs (Figure 3d). The good swelling properties of hydrogels are crucial for aligning with the wound healing process and for

https://doi.org/10.1021/acsbiomaterials.5c00072
ACS Biomater. Sci. Eng. XXXX, XXX, XXX−XXX

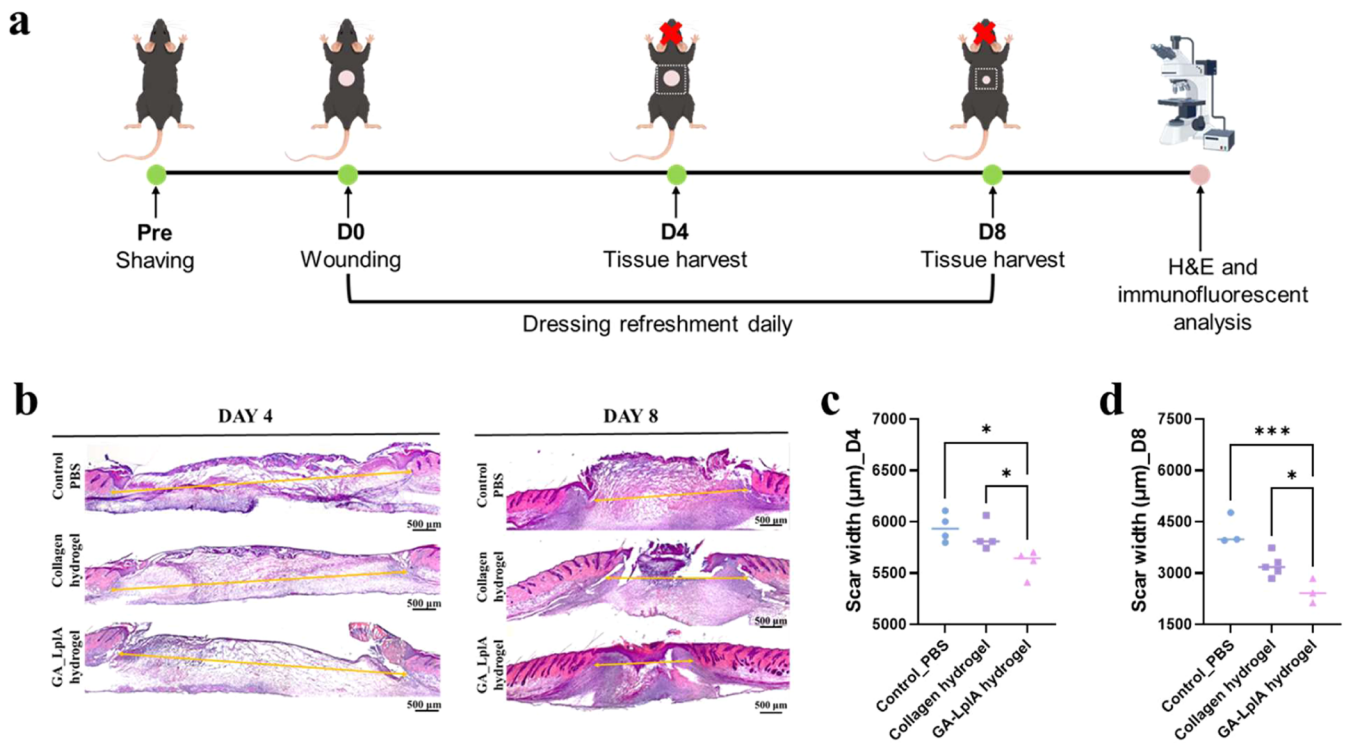

Figure 6. Hematoxylin and eosin (H&E) staining analysis of wounds treated with PBS (control group), collagen hydrogel, and GA-LplA hydrogel. (a) Illustration of wound creation and treatment timeline; (b) representative images of H&E staining of the wound tissue on day 4 and day 8. Scale bar: 500 μm; (c, d) quantitative analysis of scar widths on day 4 and day 8 ($n \geq 3$ biologically independent samples), respectively. Statistical significance was determined using a two-tailed, unpaired Student's t test. *, $p < 0.05$; **, $p < 0.01$; ***, $p < 0.001$; ns, not significant.

efficient wound exudate absorption. The GA-LplA hydrogel exhibited excellent swelling capabilities, achieving a swelling ratio of 20 (Figure S6). These characteristics make the GA-LplA hydrogel a promising candidate for biomedical applications, particularly in the areas of wound healing and tissue regeneration.

3.3. Antioxidant Properties and Reusability of the GA-LplA Hydrogel. Given that ROS can impair wound healing, ROS-scavenging hydrogels are desired for skin wound repair.[32] Serendipitously, it was found that LplA possesses catalase-mimetic activity, facilitating the decomposition of H_2O_2 into oxygen. As depicted in Figure 4a, oxygen generation correlated positively with H_2O_2 concentrations ranging from 0.5 to 20 mM. The maximum velocity (V_{max}) for LplA-catalyzed H_2O_2 decomposition was determined to be 250 μM/min/mg.

To evaluate the antioxidant potential of LplA, a ROS-induced damage model was established in L929 cells using H_2O_2, following commonly cited methods in the literature.[33] The addition of H_2O_2 at concentrations of 100 or 200 μM successfully induced an increase in intracellular ROS levels, as demonstrated by flow cytometry (Figure 4b). At a 100 μM H_2O_2 concentration, cell viability was maintained above 80%, with significant intracellular ROS accumulation observed (Figure S7). The reusability of the LplA hydrogel and GA-LplA hydrogel in the presence of H_2O_2 was also evaluated (Figure 4d,e). It was found that 100 μL of the GA-LplA hydrogel could completely degrade 1 mL of 1 mM H_2O_2 within 1 h. Furthermore, the GA-LplA hydrogel retained its activity over at least five consecutive uses. Due to limited stability, LplA hydrogel's network structure was disrupted during the fourth repetition, resulting in protein dissolution.

In terms of the cellular response, Figure 4c illustrates the impact of ROS damage on cells cultured in different hydrogels. Both the control and collagen hydrogel groups exhibited a significant increase in fluorescence intensity, indicative of ROS damage, upon exposure to 100 μM H_2O_2. Contrastingly, cells incubated with the GA-LplA hydrogel displayed resilience against H_2O_2-induced ROS damage, with fluorescence intensity remaining comparable to that of the untreated control group. These findings suggest that the GA-LplA hydrogel provides protective effects against oxidative stress and holds promise for applications in wound healing.

3.4. *In Vivo* Wound Healing Analysis. After the aforementioned evaluations, an *in vivo* full-thickness skin defect model was employed to further assess the wound closure and healing capabilities of the GA-LplA hydrogel. Figure 5a depicts the surgical procedure, dressing application, and healing timeline. As shown in Figure 5b–d, the wound areas progressively diminished in both the PBS and the GA-LplA hydrogel group on the second, fourth, sixth, and 12th days of the healing period. In the PBS group, scab formation and delayed wound closure were observed. Meanwhile, the GA-LplA treatment group exhibited a higher percentage of wound closure compared to the control group, particularly on the fourth day, with a closure rate above 70%, significantly higher than the 50% observed in the control group. This can be attributed to the antioxidant effects of GA-LplA hydrogels and their impact on cellular metabolism, which accelerated cell proliferation and reduced the duration of the inflammatory phase of wound healing.

A collagen hydrogel was incorporated into the above wound healing model experiments as a control group to prevent the acceleration of the wound healing process due to the moist

https://doi.org/10.1021/acsbiomaterials.5c00072
ACS Biomater. Sci. Eng. XXXX, XXX, XXX−XXX

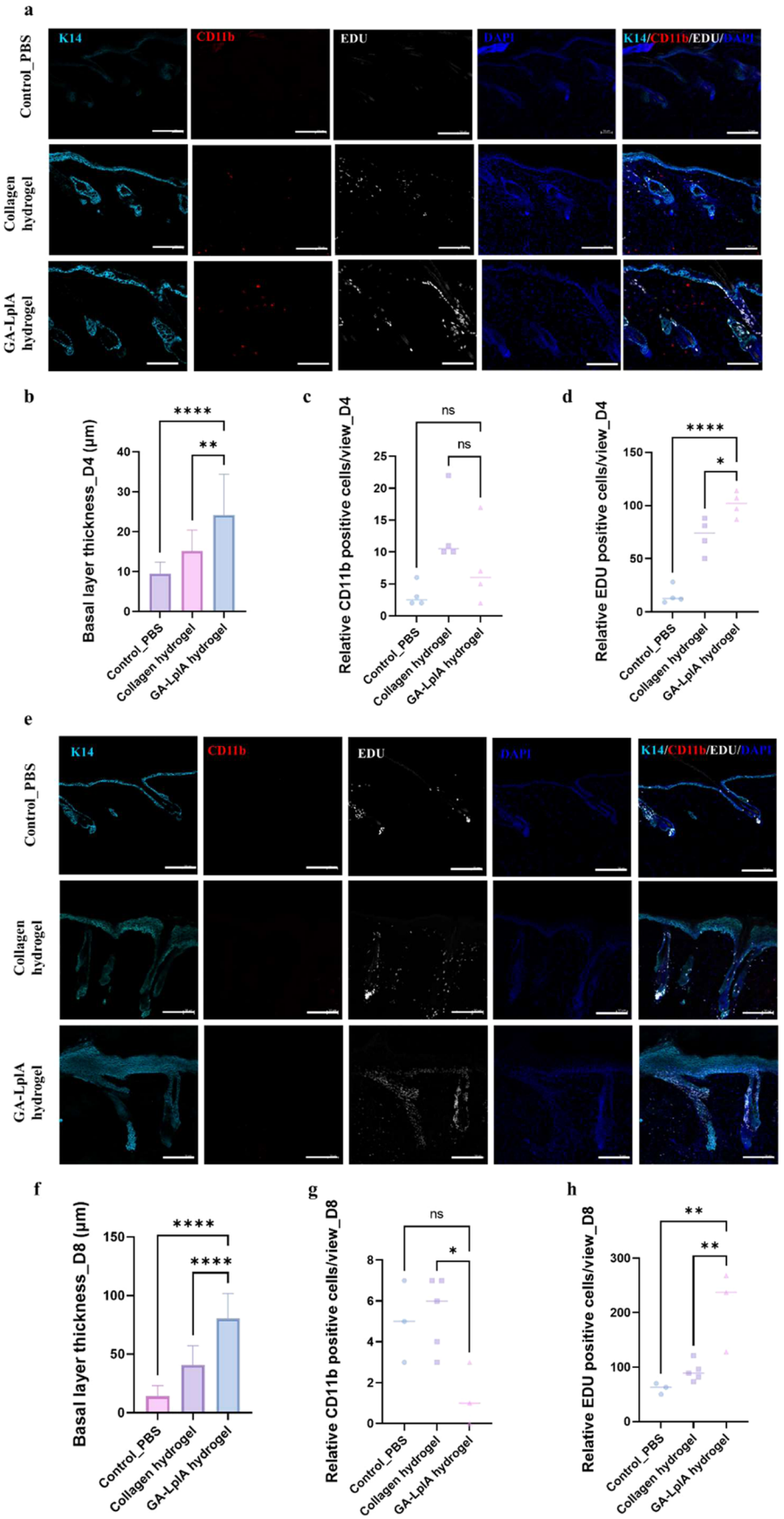

Figure 7. Immunofluorescence staining analysis of wounds that underwent treatments with the control group (PBS), collagen hydrogel group, and the GA-LplA hydrogel group. (a, e) Representative fluorescence images of K14 immunostaining (light blue), CD11b immunostaining (red), and EDU staining (white) of wound tissues on days 4 and 8 post-treatment. Cell nuclei were stained with DAPI (blue), scale bar: 200 μm; (b, f)

https://doi.org/10.1021/acsbiomaterials.5c00072
ACS Biomater. Sci. Eng. XXXX, XXX, XXX−XXX

Figure 7. continued

quantification of basal layer thickness on Day 4 and Day 8, respectively; (c, g) quantification of CD11b-positive cells on Day 4 and Day 8, respectively; and (d, h) quantification of EDU positive cells on Day 4 and Day 8, respectively. Representative images are shown from three independent experiments with similar results (a, e). Statistical significance was determined using a two-tailed, unpaired Student's *t* test. *, $p < 0.05$; **, $p < 0.01$; ***, $p < 0.001$; ns, not significant.

environment created by the GA-LplA hydrogel. Tissue samples were collected on days 4 and 8 for histopathological evaluation using hematoxylin and eosin (H&E) staining to measure the scar width. Day 4 represents a crucial time window for the inflammation and proliferation stages of the healing process, while Day 8 can reflect the regeneration stage and healing efficacy. Staining results (Figure 6b,c) showed that wound healing was slower in all treatment groups on day 4, and the scar width in the GA-LplA hydrogel group was slightly smaller than the control group and collagen hydrogel group. On the eighth day, the healing speed of every treatment group increased significantly, and a new epidermis developed (Figure 6b,d). The epidermis of the GA-LplA hydrogel group was flatter and more continuous, and the attachments, such as hair follicles and glands, increased significantly. Throughout the treatment period, all mice in the PBS, collagen hydrogel, and GA-LplA hydrogel groups exhibited normal feeding behavior and similar weight gain (Figure S8).

Epidermal regeneration was evaluated by using immunofluorescence staining to quantify key markers essential for wound closure, including the levels of cells expressing cytokeratin 14 (K14), the percentage of CD11b-positive cells, and the number of proliferating cells. These markers were used to assess the wound area's capacity for re-epithelialization, the recruitment of inflammatory factors, and cellular proliferation, respectively (Figure 7a,e). Since epithelialization is a critical indicator of complete wound healing, K14 expression, primarily expressed in hair and epithelial cells, was measured via immunofluorescence staining to evaluate re-epithelialization. Tissue staining on days 4 and 8 demonstrated that, except for the PBS group, the wound areas in both the collagen hydrogel and GA-LplA hydrogel groups were covered by keratin 14 on day 4 (Figure 7b), with enhanced K14 expression on day 8 (Figure 7f). The mean keratin 14 expression cell thickness at the wound site was used to quantify the epidermal basal layer thickness across various treatment groups. Results indicated that the GA-LplA hydrogel group exhibited a greater basal layer thickness compared to both the PBS and collagen groups, suggesting a more robust re-epithelialization capacity. Enhanced cell proliferation at the wound site promoted wound repair. Proliferating cells were quantified using EDU labeling, which revealed a greater number of labeled cells at hair follicle sites with migratory tendencies toward the wound site from day 4 onward in the GA-LplA hydrogel group (Figure 7d). By contrast, the PBS and collagen groups exhibited this trend from day 8 (Figure 7h). These findings indicate that the GA-LplA hydrogel potentially accelerates wound healing by promoting hair follicle stem cell proliferation. CD11b, a marker for various inflammatory cells, was analyzed to assess the inflammation levels. All treatment groups exhibited low inflammation levels with no significant difference in CD11b-labeled cell counts on day 4 (Figure 7c). However, there was a slight increase in immune cells in the collagen hydrogel group compared to the PBS and GA-LplA hydrogel groups on day 8 (Figure 7g). These immunofluorescence results demonstrated that the GA-LplA hydrogel did not induce an inflammatory response and accelerated wound healing by promoting re-epithelialization and cell proliferation.

4. CONCLUSIONS

In this study, a natural enzyme, LplA, with catalytic capability and self-assembly ability, has been investigated for its functions in L929 cell culture. The exogenous addition of LplA significantly increased the cellular activity by up to 150% and stimulated intracellular metabolism. However, cells aggregated into spherical clusters when using the LplA hydrogel as a cell culture matrix. To overcome this shortage, GA-LplA hydrogel was developed by cross-linking LplA with glutaraldehyde to enhance its mechanical ability. Comparative analyses revealed that the GA-LplA hydrogel outperformed both the natural LplA hydrogel and commercial collagen hydrogels in terms of cell adhesion and proliferation. Notably, the GA-LplA hydrogel substantially enhanced ROS resistance in L929 cells, suggesting its potential to effectively mitigate oxidative stress. When applied to a full-thickness skin defect mouse model, this hybrid hydrogel significantly accelerated wound healing by promoting epithelial regeneration and cell proliferation. In summary, the GA-LplA hydrogel exhibits promising characteristics, including easy preparation, enhanced cellular metabolism, proliferation, and robust resistance to ROS. These properties contribute to accelerated healing speed and significantly improved healing quality, making it a promising candidate for applications in wound healing and skin repair.

■ ASSOCIATED CONTENT

Supporting Information

The Supporting Information is available free of charge at https://pubs.acs.org/doi/10.1021/acsbiomaterials.5c00072.

SDS-PAGE analysis of the purified LplA recombinant proteins (Figure S1); Western blot analysis of LplA internalization levels in L929 cells (Figure S2); cytotoxicity assessment of hydrogels (Figure S3); pore size of hydrogels as visualized by SEM (Figure S4); injectability of GA-LplA hydrogel (Figure S5); hydrophobicity/hydrophilicity of LplA and the swelling ratio of GA-LplA hydrogel (Figure S6); ROS production in L929 cells treated with H_2O_2 (Figure S7); body weight changes in the full-thickness skin defect model (Figure S8); protein purity and endotoxin levels of LplA (Table S1); and the physicochemical properties of LplA (Table S2) (PDF)

■ AUTHOR INFORMATION

Corresponding Author

An-Ping Zeng − *Institute of Bioprocess and Biosystems Engineering, Institute of Bioprocess and Biosystems Engineering, Hamburg University of Technology, Hamburg 21073, Germany; Center of Synthetic Biology and Integrated Bioengineering, Westlake University, Hangzhou 310030 Zhejiang, China; School of Engineering, Westlake University,*

https://doi.org/10.1021/acsbiomaterials.5c00072
ACS Biomater. Sci. Eng. XXXX, XXX, XXX−XXX

Hangzhou 310030 Zhejiang, China; Research Center for Industries of the Future and Key Laboratory of Intelligent Low-Carbon Biosynthesis of Zhejiang Province, Westlake University, Hangzhou 310024 Zhejiang, China; Email: zenganping@westlake.edu.cn

Authors

Xinyi Zhang − *Institute of Bioprocess and Biosystems Engineering, Institute of Bioprocess and Biosystems Engineering, Hamburg University of Technology, Hamburg 21073, Germany; Center of Synthetic Biology and Integrated Bioengineering, Westlake University, Hangzhou 310030 Zhejiang, China;* orcid.org/0009-0004-7297-2308

Zhijuan Hu − *Center of Synthetic Biology and Integrated Bioengineering, Westlake University, Hangzhou 310030 Zhejiang, China; School of Engineering, Westlake University, Hangzhou 310030 Zhejiang, China; Research Center for Industries of the Future and Key Laboratory of Intelligent Low-Carbon Biosynthesis of Zhejiang Province, Westlake University, Hangzhou 310024 Zhejiang, China;* orcid.org/0009-0004-0571-0498

Ralf Pörtner − *Institute of Bioprocess and Biosystems Engineering, Institute of Bioprocess and Biosystems Engineering, Hamburg University of Technology, Hamburg 21073, Germany*

Complete contact information is available at: https://pubs.acs.org/10.1021/acsbiomaterials.5c00072

Author Contributions

Z.X. designed and performed the experiments, analyzed data, and wrote the manuscript. H.Z. worked with the heterologous expression of LplA in L929 and mitochondrial stress test and wrote the manuscript. Z.A.-P. conceived, designed, and supervised the project and wrote the manuscript. R.P. was involved in designing and supervising the project.

Notes

The authors declare no competing financial interest.

■ ACKNOWLEDGMENTS

This work was financially supported by the China Scholarship Council, the National Key R&D Program of China (2022YFA0912001), and the Zhejiang Key Laboratory of Low-Carbon Intelligent Synthetic Biology (2024ZY01025). The authors also acknowledge the financial support from the Westlake Education Foundation and from the Center of Synthetic Biology and Integrated Bioengineering of Westlake University. The authors thank Prof. Bing Zhang and Chao Liu for their advice and assistance with the animal experiments.

■ REFERENCES

(1) Wang, P.-H.; Huang, B.-S.; Horng, H.-C.; Yeh, C.-C.; Chen, Y.-J. Wound healing. *J. Chin. Med. Assoc.* **2018**, *81* (2), 94−101.

(2) Petkovic, M.; Mouritzen, M. V.; Mojsoska, B.; Jenssen, H. Immunomodulatory Properties of Host Defence Peptides in Skin Wound Healing. *Biomolecules* **2021**, *11* (7), No. 952, DOI: 10.3390/biom11070952.

(3) Manchanda, M.; Torres, M.; Inuossa, F.; Bansal, R.; Kumar, R.; Hunt, M.; Wheelock, C. E.; Bachar-Wikstrom, E.; Wikstrom, J. D. Metabolic Reprogramming and Reliance in Human Skin Wound Healing. *J. Invest. Dermatol.* **2023**, *143* (10), 2039−2051.e10.

(4) Casanova, A.; Wevers, A.; Navarro-Ledesma, S.; Pruimboom, L. Mitochondria: It is all about energy. *Front. Physiol.* **2023**, *14*, No. 1114231.

(5) Hunt, M.; Torres, M.; Bachar-Wikström, E.; Wikström, J. D. Multifaceted roles of mitochondria in wound healing and chronic wound pathogenesis. *Front. Cell Dev. Biol.* **2023**, *11*, No. 1252318.

(6) Yao, W. D.; Zhou, J. N.; Tang, C.; Zhang, J. L.; Chen, Z. Y.; Li, Y.; Gong, X. J.; Qu, M. Y.; Zeng, Q.; Jia, Y. L.; Wang, H. Y.; Fan, T.; Ren, J.; Guo, L. L.; Xi, J. F.; Pei, X. T.; Han, Y.; Yue, W. Hydrogel Microneedle Patches Loaded with Stem Cell Mitochondria-Enriched Microvesicles Boost the Chronic Wound Healing. *ACS Nano* **2024**, *18* (39), 26733−26750.

(7) Sarojini, H.; Bajorek, A.; Wan, R.; Wang, J.; Zhang, Q.; Billeter, A. T.; Chien, S. Enhanced Skin Incisional Wound Healing With Intracellular ATP Delivery via Macrophage Proliferation and Direct Collagen Production. *Front. Pharmacol.* **2021**, *12*, No. 594586.

(8) Sarojini, H.; Billeter, A. T.; Eichenberger, S.; Druen, D.; Barnett, R.; Gardner, S. A.; Galbraith, N. J.; Polk, H. C., Jr.; Chien, S. Rapid tissue regeneration induced by intracellular ATP delivery-A preliminary mechanistic study. *PLoS One* **2017**, *12* (4), No. e0174899.

(9) Jiang, Y.; Feng, X.; Qiao, X.; Li, Y.; Li, X.; Yang, J.; Han, L. Plant-inspired visible-light-driven bioenergetic hydrogels for chronic wound healing. *Bioact. Mater.* **2024**, *41*, 523−536.

(10) Hao, R.; Cui, Z.; Zhang, X.; Tian, M.; Zhang, L.; Rao, F.; Xue, J. Rational Design and Preparation of Functional Hydrogels for Skin Wound Healing. *Front. Chem.* **2021**, *9*, No. 839055.

(11) Li, Y.; Wang, Y.; Ding, Y.; Fan, X.; Ye, L.; Pan, Q.; Zhang, B.; Li, P.; Luo, K.; Hu, B.; He, B.; Pu, Y. A Double Network Composite Hydrogel with Self-Regulating Cu(2+)/Luteolin Release and Mechanical Modulation for Enhanced Wound Healing. *ACS Nano* **2024**, *18* (26), 17251−17266.

(12) Chu, B.; He, J. M.; Liu, L. L.; Wu, C. X.; You, L. L.; Li, X. L.; Wang, S.; Chen, C. S.; Tu, M. Proangiogenic Peptide Nanofiber Hydrogels for Wound Healing. *ACS Biomater. Sci. Eng.* **2021**, *7* (3), 1100−1110.

(13) Chakrabarti, S.; Mazumder, B.; Rajkonwar, J.; Pathak, M. P.; Patowary, P.; Chattopadhyay, P. bFGF and collagen matrix hydrogel attenuates burn wound inflammation through activation of ERK and TRK pathway. *Sci. Rep.* **2021**, *11* (1), No. 3357.

(14) Yao, Y.; Zhang, A.; Yuan, C.; Chen, X.; Liu, Y. Recent trends on burn wound care: hydrogel dressings and scaffolds. *Biomater. Sci.* **2021**, *9* (13), 4523−4540.

(15) Green, D. E.; Morris, T. W.; Green, J.; Cronan, J. E., Jr.; Guest, J. R. Purification and properties of the lipoate protein ligase of *Escherichia coli*. *Biochem. J.* **1995**, *309* (Pt 3), 853−862.

(16) Fujiwara, K.; Maita, N.; Hosaka, H.; Okamura-Ikeda, K.; Nakagawa, A.; Taniguchi, H. Global conformational change associated with the two-step reaction catalyzed by *Escherichia coli* lipoate-protein ligase A. *J. Biol. Chem.* **2010**, *285* (13), 9971−9980.

(17) Cronan, J. E. Lipoic acid attachment to proteins: stimulating new developments. *Microbiol. Mol. Biol. Rev.* **2024**, *88* (2), No. e00005-24.

(18) Cao, X.; Koch, T.; Steffens, L.; Finkensieper, J.; Zigann, R.; Cronan, J. E.; Dahl, C. Lipoate-binding proteins and specific lipoate-protein ligases in microbial sulfur oxidation reveal an atpyical role for an old cofactor. *eLife* **2018**, *7*, No. e37439, DOI: 10.7554/eLife.37439.

(19) Bick, N. R.; Dreishpoon, M. B.; Perry, A.; Rogachevskaya, A.; Bottomley, S. S.; Fleming, M. D.; Ducamp, S.; Tsvetkov, P. Engineered bacterial lipoate protein ligase A (lplA) restores lipoylation in cell models of lipoylation deficiency. *J. Biol. Chem.* **2024**, *300* (12), No. 107995.

(20) Hu, Z.; Yu, J.; Liu, Z.; Jiang, M.; Zeng, A.-P. Bacterial lipoate protein ligases rescue lipoylation and respiration deficiency in mammals *bioRxiv* 2024, *1122* .

(21) Nie, J.; Zhang, X.; Wang, W.; Ren, J.; Zeng, A. P. Tunable Protein Hydrogels: Present State and Emerging Development. *Adv. Biochem. Eng./ Biotechnol.* **2021**, *178*, 63−97.

(22) Nie, J.; Zhang, X.; Hu, Z.; Wang, W.; Schroer, M. A.; Ren, J.; Svergun, D.; Chen, A.; Yang, P.; Zeng, A. P. A globular protein exhibits rare phase behavior and forms chemically regulated

orthogonal condensates in cells. *Nat. Commun.* **2025**, *16* (1), No. 2449.
(23) Wang, Y.; Jiang, J.; Xiong, Q.; Li, S.; Shao, J.; Xie, M.; Zeng, A. P. Programmable solid-state condensates for spatiotemporal control of mammalian gene expression *Nat. Chem. Biol.* 2025 DOI: 10.1038/s41589-025-01860-0.
(24) Zhang, X.; Nie, J.; Zheng, Y.; Ren, J.; Zeng, A. P. Activation and competition of lipoylation of H protein and its hydrolysis in a reaction cascade catalyzed by the multifunctional enzyme lipoate-protein ligase A. *Biotechnol. Bioeng.* **2020**, *117* (12), 3677−3687.
(25) Muir, V. G.; Burdick, J. A. Chemically Modified Biopolymers for the Formation of Biomedical Hydrogels. *Chem. Rev.* **2021**, *121* (18), 10908−10949.
(26) Lynch, A. M.; Wilcox, P. Review of the performance of the 3T3 NRU in vitro phototoxicity assay in the pharmaceutical industry. *Exp. Toxicol. Pathol.* **2011**, *63* (3), 209−214.
(27) O'Brien, J.; Wilson, I.; Orton, T.; Pognan, F. Investigation of the Alamar Blue (resazurin) fluorescent dye for the assessment of mammalian cell cytotoxicity. *Eur. J. Biochem.* **2000**, *267* (17), 5421−5426.
(28) Weyermann, J.; Lochmann, D.; Zimmer, A. A practical note on the use of cytotoxicity assays. *Int. J. Pharm.* **2005**, *288* (2), 369−376.
(29) Nie, J.; Zhang, X.; Liu, Y.; Schroer, M. A.; Wang, W.; Ren, J.; Svergun, D. I.; Zeng, A.-P. A non-structural pure enzyme protein forms a LCST type of stimuli-responsive and reversible hydrogel with novel structure and catalytic activity. *bioRxiv* **2021**, DOI: 10.1101/2021.02.07.430034.
(30) Discher, D. E.; Janmey, P.; Wang, Y. L. Tissue cells feel and respond to the stiffness of their substrate. *Science* **2005**, *310* (5751), 1139−1143.
(31) Pelham, R. J., Jr.; Wang, Y. Cell locomotion and focal adhesions are regulated by substrate flexibility. *Proc. Natl. Acad. Sci. U.S.A.* **1997**, *94* (25), 13661−13665.
(32) Han, X.; Ju, L. S.; Irudayaraj, J. Oxygenated Wound Dressings for Hypoxia Mitigation and Enhanced Wound Healing. *Mol. Pharmaceutics* **2023**, *20* (7), 3338−3355.
(33) Fan, X.; Zhang, Z.; Gao, W.; Pan, Q.; Luo, K.; He, B.; Pu, Y. An Engineered Butyrate-Derived Polymer Nanoplatform as a Mucosa-Healing Enhancer Potentiates the Therapeutic Effect of Magnolol in Inflammatory Bowel Disease. *ACS Nano* **2024**, *18* (1), 229−244.

https://doi.org/10.1021/acsbiomaterials.5c00072
ACS Biomater. Sci. Eng. XXXX, XXX, XXX−XXX